Available online at www.sciencedirect.com

ScienceDirect

Procedia CIRP 82 (2019) 267–272

www.elsevier.com/locate/procedia

17th CIRP Conference on Modelling of Machining Operations

Numerical Investigation of Orthogonal Cutting Processes with Tool Vibration of Ti6Al4V Alloy

Fei Shuang [a, b] and Wei Ma [a*]

[a] Institute of Mechanics, Chinese Academy of Sciences, Beijing 100190, China
[b] Department of mechanical and Aerospace Engineering, University of Florida, Gainesville, FL 32611-6250, USA

* Corresponding author. Tel.: 86+01-82544238; fax: 86+01-82544238. *E-mail address:* watwm@imech.ac.cn

Abstract

This article investigates the vibration cutting process of Ti6Al4V alloy numerically and theoretically. The Coupling Eulerian-Lagrangian finite element models with one-tool and double-tool are established, to simulate the cutting processes with tool forced vibration and self-exited vibration respectively. It is shown that low-frequency forced vibration aggravates the periodic shear banding instability and increases the cutting force amplitude, whereas high-frequency forced vibration can improve the machined quality. Furthermore, the self-exited vibration due to fluctuating cutting thickness with low frequency promotes the shear banding evolution in chip. The self-exited vibration stability limit is found dependent on the frictional behavior, penetration resistance and the inherent vibration sources of tool-workpiece system. These simulation results show good agreement with theoretical models, which provide practical guidelines for improving vibration machining.

Peer-review under responsibility of the scientific committee of The 17th CIRP Conference on Modelling of Machining Operations

Keywords: vibration cutting; shear banding instability; wavy machined surface forced vibration, self-excited vibration, stability limit

1. Introduction

Two types of vibration phenomena in cutting attract attention of researchers. The first one is *forced vibration* (FV) of tool which is caused by external excitations of tool-workpiece system. The adverse effects of FV on cutting process can be alleviated and utilized. For example, the vibration assisted machining technologies have exhibited the superior machining performances [1-3] since they can improve the machining quality evidently [4] by reducing cutting forces [5], increasing tool life [6], and enhancing cutting stability [7]. Especially, they have been successfully applied to the precision machining of various difficult-to-cut materials [8, 9].

The second is *self-excited vibration* (SEV) resulting from internal excitations [10, 11], which brings destructive effects to the machine tool and influences machining quality [12, 13]. Therefore, how to effectively control and further make use of SEV in cutting is a pressing issue facing the academic and engineering communities at present. In the SEV cutting, if the cut depth is larger than the stability limit, the cutting process becomes unstable [14]. The stability limit is related to the cutting depth and the chip width [15] which depends on the dynamics of tool-workpiece system, cutting conditions and tool geometry [16, 17]. The ultrasonic vibration of tool can increase the stability of vibration cutting process (VCP) [18, 19].

During the past decades, decisive progress has been made in the effects of vibration phenomenon on the continuous chip formation while the serrated and discontinuous chip is rarely involved. As an internal vibration source, the periodic shear banding instability (PSBI) in serrated chip makes the vibration cutting problem more complicated. Then, how does the tool vibration influence the chip formation mechanism in the FV cutting process? And how does the oscillation phenomenon caused by the PSBI behavior and the machined wavy surface affect the cutting process? The causalities of these issues are not yet clarified and will be addressed numerically and theoretically

2212-8271 © 2019 The Authors. Published by Elsevier B.V.
Peer-review under responsibility of the scientific committee of The 17th CIRP Conference on Modelling of Machining Operations
10.1016/j.procir.2019.04.032

in this article. The aim is to provide an effective numerical method for modelling VCP of metals and to reveal the influence of PSBI and the varying cut thickness on the cutting process.

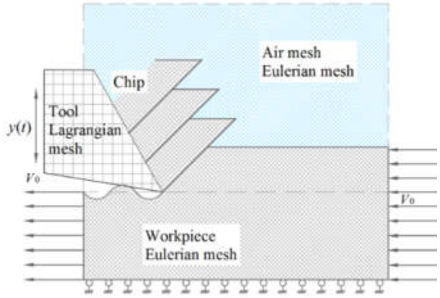

Fig. 1. The CEL model for modeling the metal cutting process and the FE mesh arrangement.

2. Coupling Eulerian-Lagrangian finite element model

In the simulation of metal cutting process with Lagrangian finite element method (LFEM), a predefined parting line, along which chip separation occurs, is needed with a failure criterion. The shear failure criterion, for example, must be introduced [20] to remove failure elements. In addition, low mesh quality due to the severe element distortion has a detrimental effect on the accuracy and terminates the simulation quickly. In modelling with the Eulerian formulation, the parting line and failure criterion are not required, but the chip shape needs to be known in advance. These limitations make the two techniques ill-suited for modelling the cutting processes with tool vibration or having blunt edge since such line cannot be preset in these cases [21]. The Coupling Eulerian-Lagrangian (CEL) finite element (FE) model, however, is established based on the principle of computational fluid mechanics, which has the advantages of Lagrangian and Eulerian techniques and overcomes their drawbacks. Therefore, it is suitable for numerical simulation of cutting process with tool vibration [22]. This model constitutes the foundation of the numerical analysis of vibration cutting mechanism in this article.

Fig. 1 shows the CEL model for the simulation of orthogonal cutting process (OCP) and the FE mesh arrangement. In this model, Lagrangian mesh is attached to the rigid tool and Eulerian mesh is fixed in spatial. The latter is used to describe the motion and deformation of workpiece and chip materials. Moreover, the air mesh provides sufficiently large room for the growth of chips. During simulations, the tool is fixed and the workpiece is constrained to move in negative x-axial direction. The boundary conditions with a constant horizontal cutting speed and zero vertical speed are imposed on the outer surfaces of workpiece. The chips with various shape enter the air mesh area. The unconstrained flow of chip on the free boundary is controlled by the volume approach of solid [23]. Since the CEL model has eliminated the limitation of the preset separation line and the influence of the mesh distortion, it is convenient to simulate the VCP and the chip formation with various morphologies at different cutting speeds. The detailed descriptions of the CEL model in the simulation of the VCP is given in the reference [24].

The work-material of Ti6Al4V alloy is assumed to be isotropic and thermo-viscoplastic. The Johnson-Cook (J-C) law describes the plastic flow in cutting which has the form [25]

$$\sigma_{eq}^{p}=\left[A_0+B_0\left(\varepsilon_{eq}^{p}\right)^{n}\right]\left(1+C_0\ln\frac{\dot{\varepsilon}_{eq}^{p}}{\dot{\varepsilon}_0}\right)\left[1-\left(\frac{T-T_0}{T_m-T_0}\right)^{m}\right] \quad (1)$$

where σ_{eq}^{p} is the equivalent stress, ε_{eq}^{p} the equivalent plastic strain, $\dot{\varepsilon}_{eq}^{p}$ the plastic strain rate, $\dot{\varepsilon}_0$ the reference strain rate. T is the current temperature, T_0 the room temperature, T_m the melting temperature. A_0, B_0, C_0, m and n are J-C constitution parameters. The plastic flow of work-material is governed by J_2 flow-law. The material properties and constitutive parameters of Ti6Al4V alloy is given in Table 1. The cutting simulations are performed in commercial ABAQUS software.

3. Forced-vibration cutting process

In VCP, the tool vibration changes the plastic flow stability of chip material, and conversely, the PSBI behavior affects the vibration motion of tool system. The former as the FV cutting process will be considered in this section. The latter as the SEV process of tool will be studied in the next section.

Table 1. Material properties and constitutive parameter of Ti6Al4V alloy a tool [25].

Properties *Symbol* (Unit)	Ti6Al4V alloy	Tool
Density ρ (kg/m^3)	4430	11900
Elastic modulus E (GPa)	114	630
Poisson's ratio v	0.342	0.26
Specific heat c (J/kg·K)	520	334
Thermal conductivity λ (W/m·K)	6.7	100
Expansion coefficient α (K^{-1})	9.2×10^{-6}	5.4×10^{-6}
Melting temperature T_m (K)	1873	
Fraction	0.9	
Friction coefficient μ	0.4	

Material parameters Symbol (Unit)	Values
A_0 (MPa)	725
B_0 (MPa)	683
n	0.47
C_0	0.035
m	1
$\dot{\varepsilon}_0$	10^{-3}

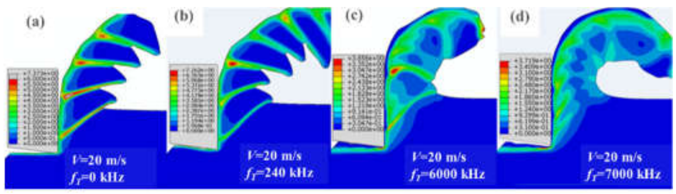

Fig. 2. The effect of tool FV frequency on the chip morphology in cutting process with the cutting speed of 20 m/s.

3.1 Simulation of forced vibration cutting

To study the FV cutting process, a single-free degree model is proposed (Fig. 1). The cutting conditions are given as the cut thickness 100 μm, rake angle 0° and the cutting speeds 20 m/s. The tool vibration is set in y-axial direction according to $y(t)=A_0\sin2\pi f_T t$, where A_0=10 μm is the amplitude and f_T is the frequency of tool FV.

Simulations with various FV frequency were carried out when cutting speed is 20 m/s. The chip morphologies and equivalent strain contour are shown in Fig. 2. When the frequency of tool is zero (Fig. 2a), the serrated chip forms and the PSBI frequency is determined as 240 kHz. When the tool FV frequency equals 240 kHz (Fig.2b), the segmentation intensity increases, indicating that low-frequency FV promotes the PSBI evolution. When the tool vibrates at high frequency (Fig. 2c and d), the shear bands disappear and the serrated chips changes into the continuous ones, implying that high-frequency FV suppresses the PSBI evolution and there must exist a critical frequency of the tool FV denoting the transition of chip morphology.

Fig. 3 illustrates the dependence of PSBI frequencies and the transition frequencies of chip morphology on cutting speeds. The region above the transition frequency curve denotes stable plastic flow of continuous chip. However, it represents the unstable plastic flow of serrated chip without vibration. This demonstrates that the high-frequency FV of tool leads to the stable plastic flow of chip material.

Fig. 4 shows the simulation cutting forces. The oscillation frequency of cutting force is identical with the PSBI frequency without FV (Fig. 4a). As f_T=240 kHz, that is, resonance frequency, the vibration amplitude of cutting force gets enhanced (Fig. 4b). As f_T=6000 kHz that is considered as the transition frequency, the low-frequency component of cutting force begins to disappear (Fig. 4c) and as f_T=7000 kHz, it disappears completely (Fig. 4d). The serrated chip fully turns into continuous finally.

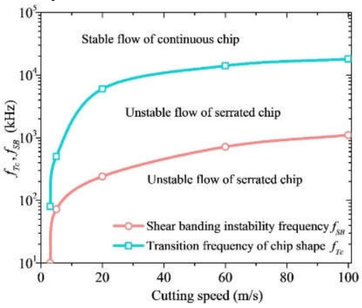

Fig. 3. The dependence of the PSBI frequency f_{SB} and the transition frequency of chip shape f_T on the cutting speeds. (图中最下"unstable flow of serrated chip"是否有误？)

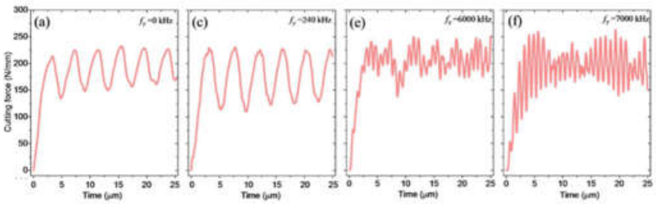

Fig. 4. The effects of tool FV frequencies on the cutting forces as V=20 m/s.

3.2 Analysis of chip flow stability

The tool FV induces the oscillations of shear stress in primary shear zone (PSZ) and pressure on the tool-chip interface, and further changes the chip formation mechanism. A linear stability analysis on chip flow is performed to clarify this causality. The shear stress component is assumed as $\tau_0=\tau'+\tau''\sin(2\pi f_T t+\varphi)$, where t is time, τ' is the shear stress without vibration, τ'', f_T and φ are the amplitude, frequency and initial phase angle. According to the analysis in [25], the criterion for evaluating the stability of chip flow is obtained

$$F_{Inst}=I_1+I_2+I_3>1 \tag{4}$$

where

$$I_1=\frac{\tau_0\beta P_0}{\rho c Q_0}, I_2=\frac{\tau'\sin(2\pi f_T t+\phi)\beta P_0}{\rho c Q_0}, I_3=-\frac{2\sqrt{\dot{p}_{N0}}\cos(2\pi f_T t+\phi)\beta P_0}{\rho c Q_0} \tag{5}$$

$$\dot{p}_{N0}=2\pi f_T\tau'\rho c R_0$$

In (5), Q_0, R_0 and P_0 represent the strain hardening, strain rate sensitivity and thermal softening of material respectively. The terms in the nominators represents the thermal softening effect and the denominator demotes the strain hardening effect. Thus, if the value of function F_{Inst} in (4) is greater than one, the plastic flow is possibly unstable; otherwise, it is stable. Here, I_1 describes the PSBI behavior, and I_2 and I_3 denote the influences of the shear stress and pressure oscillations on the shear banding evolution accordingly.

The analytical results are shown in Fig. 5 and the curve in Fig. 5a corresponds to PSBI as f_T=0 kHz (Fig. 2a). In the low-frequency FV cutting process, fluctuating shear stress promotes the shear banding evolution since the PSBI amplitude increases evidently but the frequency remains unchanged (Fig. 5b). Pressure oscillation restrains the evolution of shear bands to some extent as demonstrated by a decreased amplitude of partial shear banding oscillation (Fig. 5c). In the high-frequency cutting, fluctuating shear stress still hasn't induced the change of the PSBI behavior besides the information of high-frequency oscillation as shown in these curves (Fig. 5d). When the pressure oscillation is considered, the PSBI phenomenon disappears completely, implying that the continuous chip has fully developed (Fig. 5e). In the FV cutting, the work done by tool on workpiece turns into the shear localized deformation energy of the PSZ material, and thus, the shear stress oscillation intensifies the material softening effect within shear bands and facilitates the PSBI behavior. However, the high-frequency pressure oscillation transfers some shear deformation energy required by the shear banding evolution into the tensile deformation energy of cutting edge material, which weakens the material softening phenomenon within shear bands. This forcefully restrains the shear banding evolution and results in the transition of the serrated chip into the continuous chip.

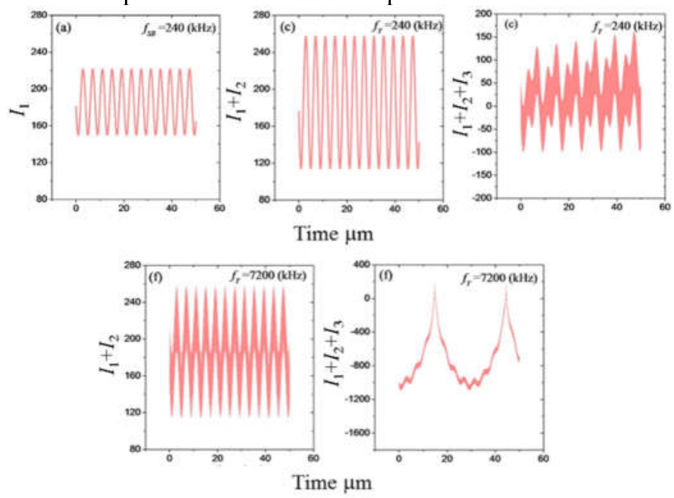

Fig. 5 The variation curves of different term combinations of the functions F_{Inst} with time.

4. Self-exited vibration cutting process

4.1 Simulation of self-exited vibration cutting process

To simulate the SEV cutting process, a double-tool CEL FE model is designed (Fig. 6). This model assumes that the two tools have same mass, stiffness, damping and geometrical features. The tool-1 FV represents the structural dynamics of tool system. The tool-2 SEV in y-axial direction is induced by two vibration sources, i.e., the wavy machined surface and the

PSBI in high-speed cutting. Two tools have same cutting speed and keep the constant spacing in cutting process. The wavy surface is induced by tool-1 FV cutting and described by $y_1=y_{10}+A_{w1}\sin(2\pi f_{T1}t+\theta_{w1})$, where y_1 denotes the vertical oscillation displacement at time t, f_{T1} the vibration frequency, θ_{w1} the initial phase angle and A_{w1} the vibration amplitude. The average cut depth is y_{10}=100 μm and the cutting speed is V=20 m/s. Under these cutting conditions, the plastic flow of chip is unstable and leads to the formation of serrated chip (Fig. 7).

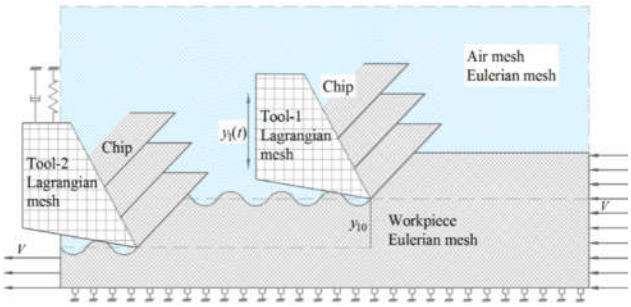

Fig. 6. The double-tool FE model for the simulation of the tool SEV cutting process.

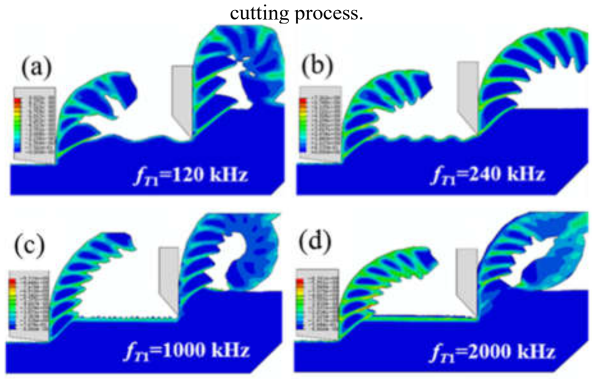

Fig. 7. The contours of equivalent plastic strain under different vibration frequency of tool-1 (V=20 m/s).

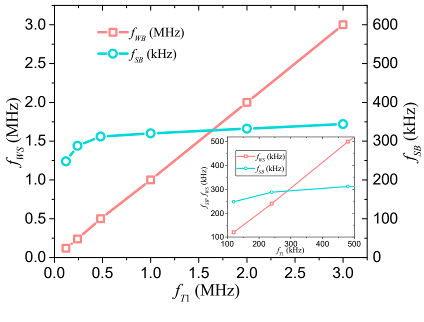

Fig.8. The relationships among the frequencies of the tool-1 FV, the wavy surface oscillation and the PSBI in the SEV cutting process.

The SEV cutting forces and ploughing forces depend on the FV frequency (Fig. 9). For low f_{T1}, the cutting force gets into an unstable oscillation state in amplitude. Both the average cutting forces and the f_{SB} change slightly with increasing f_{T1}(Fig. 9a and b). When f_{T1} is high, the oscillation frequency of cutting force rises evidently due to the increasing f_{SB} (Fig. 9c and d), which are consistent with the simulation results in Fig 7. Therefore, the dominant influences of the wavy surface and the PSBI on the SEV cutting process occur respectively in different ranges of f_{T1}. Moreover, the relative phase difference of the cutting force is opposite to that of ploughing force and displacement.

In the SEV cutting, the wavy surface generates varying cut thicknesses. For low f_{T1}, the wavelength of wavy surface is greater than shear band spacing, so that multiple shear bands can form within the cutting distance of a wavelength and the larger/smaller the chip thickness, the longer/shorter the shear band (Fig. 7a and b). As f_{T1} is higher, the PSBI frequency f_{SB} increases with f_{T1} and the serrated chip tends to have uniform segmentation due to homogeneous chip thickness (Fig. 7c and d). The frequency relationship summarized in Fig. 8 indicates that the wavy surface frequency f_{WB} is linearly proportional to f_{T1} and f_{SB} is only sensitive to lower f_{T1}.

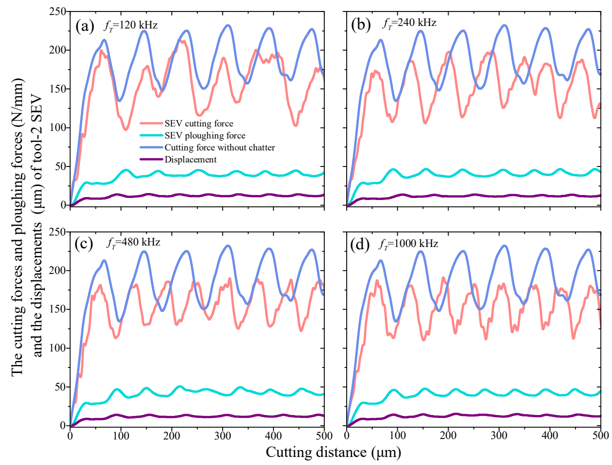

Fig. 9. The cutting forces and ploughing forces of tool-2 SEV vary with the cutting time (V = 20 m/s).

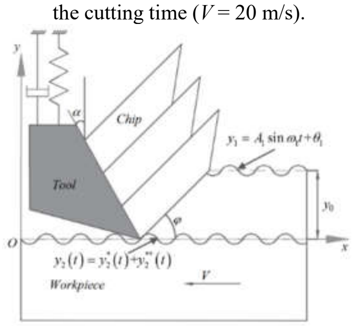

Fig. 10. The analytical model of the cutting process with tool-2 SEV motion.

4.2 Stability analysis of self-exited vibration cutting process

A spring-mass-damper system with single degree of freedom models the SEV cutting process (Fig. 10). The average cut depth, the rake angle and the shear angle are denoted by y_0, α and φ, respectively. Assume that the tool system has the equivalent mass m_0, constant equivalent stiffness k_0 and damping coefficient μ_0. The forces of the tool-2 acting on the chip and workpiece include the cutting force F_y and the ploughing force f_y. A stationary coordinate system xOy is attached to the symmetry plane of the tool-workpiece machine system. $y_2(t)$ represents the transient vertical position of the tool-2 edge at time t. If the assumption of small amplitude vibration is used, the equation of motion can be written as [26, 27]:

$$m_0\ddot{y}_2 + \mu_0\dot{y}_2 + k_0 y_2 = \left(-F_y\right) + \left(-f_y\right) \tag{6}$$

where

$$F_y = -\frac{(y_1 - y_2)w\tau\sin(\beta-\alpha)}{\sin\varphi\cos(\varphi+\beta-\alpha)},\; f_y = \frac{\mu_c w}{V}\dot{y}_2 \tag{7}$$

where $\tau=\tau_0+A_{s0}\sin(\omega_s+\theta_s)$ is the shear stress on the shear plane, τ_0 is the mean shear stress, A_{s0} the oscillation amplitude of shear stress, ω_s the angular velocity of PSBI and θ_s the initial phase angle. $\beta=\tan^{-1}(\mu)$ is the friction angle, μ is the friction coefficient of the tool-chip interface, w is the cut width, μ_c is the cutting damping coefficient and $\alpha=0°$. Thus, the undulation of the wavy surface with the average cut depth y_0 is described as $y_1=y_0+A_{w0}\sin(\omega_w+\theta_w)$, where A_{w0} denotes the oscillation amplitude, ω_w the angular velocity and θ_w the initial phase angle. The shear stress in PSZ varies with PSBI and wavy surface oscillation.

By insetting equation (7) into (6) and only the linear terms remain, the governing equation is given as:

$$\ddot{y}_2+2\Xi\Omega_n\dot{y}_2+\Omega_n^2y_2=C_0\left[1+A_w\sin\left(\omega_w t+\theta_w\right)\right]\left[1+A_s\sin\left(\omega_s t+\theta_s\right)\right] \quad (8)$$

where the equivalent relative damping coefficient Ξ and the equivalent angular velocity Ω_n are introduced as follows:

$$2\Xi\Omega_n=2\xi\omega_n-\frac{\mu_c w}{m_0 V},\Omega_n^2=\omega_n^2-\frac{C_0}{y_0},A_w=\frac{A_{w0}}{y_0},A_s=\frac{A_{s0}}{\tau_0}$$
$$2\zeta\omega_n=\frac{\mu_0}{m_0},\omega_n^2=\frac{k_0}{m_0},C_0=\frac{y_0\tau_0 w\sin\beta}{m_0\sin\varphi\cos(\varphi+\beta)} \quad (9)$$

In (9), ξ and ω_n are relative damping coefficient and the inherent angular velocity. In the derivation of equation (8), the influence of shear stress oscillation on the equivalent angular velocity Ω_n has been neglected. The completed solution of equation (8) is found as

$$y_2(t)=y_2^*(t)+y_2^{**}(t)$$
$$y_2^*(t)=C_1e^{\omega^+t}+C_2e^{\omega^-t} \quad (10)$$
$$y_2^{**}(t)=\frac{C_0}{\Omega_n^2}+\sum_{i=1}^{2}\left[\Psi_i\sin\left(\omega_{\Pi_i}t+\Theta_{\Pi_i}\right)+(-1)^{i+1}\Psi_{i+2}\cos\left(\omega_{\Pi_{i+2}}t+\Theta_{\Pi_{i+2}}\right)\right]$$

where

$$\omega^+=-\Omega_n\left(\Xi+\sqrt{\Xi^2-1}\right),\omega^-=-\Omega_n\left(\Xi-\sqrt{\Xi^2-1}\right)$$
$$C_1=\frac{\omega^-y_2^*(0)+\dot{y}_2^{**}(0)}{2\Xi\Omega_n},C_2=\frac{\omega^+y_2^{**}(0)-\dot{y}_2^{**}(0)}{2\Xi\Omega_n} \quad (11)$$
$$\Psi_1=\frac{C_0A_{\Pi_1}}{\Gamma_1},\Psi_2=\frac{C_0A_{\Pi_2}}{\Gamma_2},\Psi_3=\frac{C_0A_{\Pi_1}A_{\Pi_2}}{2\Gamma_3},\Psi_4=\frac{C_0A_{\Pi_1}A_{\Pi_2}}{2\Gamma_4}$$
$$\Gamma_i=\sqrt{\left(\Omega_n^2-\omega_{\Pi_i}^2\right)^2+\left(2\Xi\Omega_n\omega_{\Pi_i}\right)^2},\omega_{\Pi_3}=\omega_{\Pi_1}-\omega_{\Pi_2},\omega_{\Pi_4}=\omega_{\Pi_1}+\omega_{\Pi_2}$$
$$\Theta_{\Pi_i}=\theta_{\Pi_i}-\theta_{\omega\Pi_i},\theta_{\Pi_3}=\theta_{\Pi_1}-\theta_{\Pi_2},\theta_{\Pi_4}=\theta_{\Pi_1}+\theta_{\Pi_2},\theta_{\omega\Pi_i}=\arctan\left|\frac{2\Xi\Omega_n\omega_{\Pi_i}}{\Omega_n^2-\omega_{\Pi_i}^2}\right|$$

where Π_i (i=1,2,…4) stand for w, s, w-s and w+s, respectively, and the subscripts w and s denote the wavy surface and the shear bands respectively. Θ_{Π_i} is the equivalent phase difference.

The solution (10) shows that the SEV consists of four modes induced by the wavy surface and PSBI, and their coupled effects. The displacement-time curves are shown in Fig. 11. The parameters used are listed in Table 2. The results demonstrate a good agreement between the modeling and analytical results in both low and high damping cases. The influence of Ξ on the SEV stability is significant. When it is sufficiently large, the SEV disappears, otherwise, the SEV occurs. The frequency of tool-2 displacement due to SEV is closer to f_{SB}, implying that the PSBI behavior governs the SEV process and the influence of wavy surface is not significant.

The additional cutting damping $2\Xi\Omega_n$ between the tool edge and adjacent flank face exerts obvious influence on the SEV stability. The displacement-time curves (Fig. 12) illustrate that, as $2\Xi\Omega_n=10^5$ N/m, the SEV is stable if w<10 μm and as w>50 μm, the SEV starts to enter into unstable state (Fig 12a). As $2\Xi\Omega_n=10^4$ N/m, the amplitude of SEV increases dramatically as the cutting width increases. As w=50 μm, the SEV gets into unstable state (Fig. 12b). This unstable SEV process is a typical phenomenon observed in the vibration cutting tests [28].

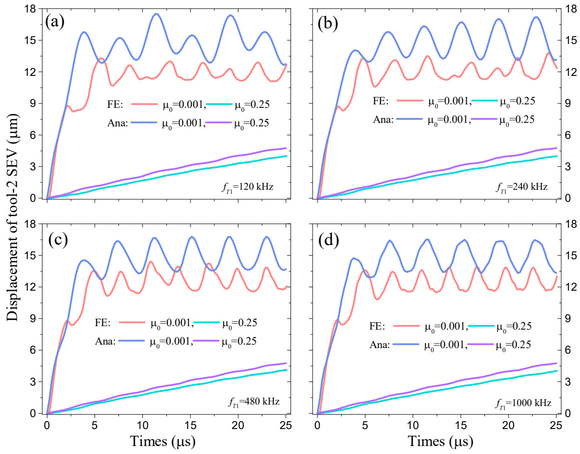

Fig. 11. The tool-2 SEV displacement-time curves at different relevant damping coefficients ($\theta_w=\theta_s=0$, V=20 m/s).

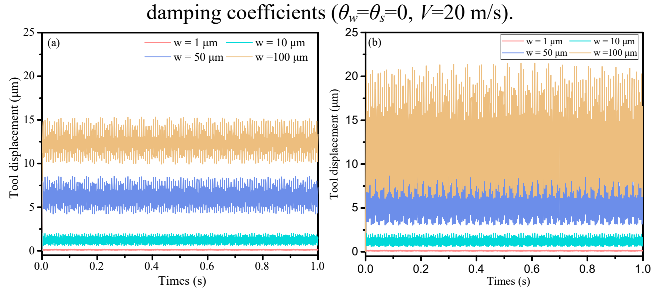

Fig. 12. The effect of the additional damping in cutting on the tool SEV at different cutting widths (a) $\mu_c=10^5$ N/m, (b) $\mu_c=10^4$ N/m.

Table 2. The parameters used in the present analysis [8].

Name(Unit)	Symbol	Value
Mass (kg)	m_0	0.36
Damping (N s/m)	μ_0	0.001, 0.25
Damping coefficient (N/m)	μ_c	10^4, 10^5, 10^6
Cutting speed (m/s)	V	20
System stiffness (N/m)	k_0	4000
Width of cutting (μm)	w	1, 10, 100
Friction angle (rad)	β	0.12
Shear angle (rad)	φ	π/4
Cutting thickness (μm)	y_0	100
Amplitude (μm)	A_w	10
Wave surface frequency (kHz)	ω_w	100-3000
Shear stress (Pa)	τ_0	0.37×10^8
Amplitude of shear stress (Pa)	A_s	$0.3\tau_0$
Shear band frequency (kHz)	ω_s	240

5. Conclusions

In this work, the CEL FE model is successfully used to simulate the FV and SEV cutting processes. The theoretical models are also established, and corresponding analytic results show good agreement with simulation results. Several major findings are summarized as follows:

(i) The simulations demonstrate that the low-frequency FV assists the unstable flow of material in the serrated chip, and the strongest impacting on the chip morphology and the cutting force presents at the resonance frequency. The high-frequency

FV suppresses the PSBI evolution, resulting in the transition of the serrated chip into the continuous chip. Since the transition frequency is unattainable in practical applications, the vibration assisted machining with the low-frequency FV may worsen the negative effect of PSBI and the high-frequency FV can be considered as a potential technology to improve machined surface quality effectively.

(ii) The linear stability analysis on the FV cutting process gives the reasonable interpretations that how FV frequency influences the mechanisms of the chip formation and shape transition. The oscillation of shear stress doesn't affect the PSBI frequency and formation mechanism, but induces high-frequency vibration of material points in the shear bands, which results in the further homogenization of shear deformation energy distribution. The influence of pressure oscillation emerges at the stage of high-frequency vibration through transferring some shear deformation energy into the tensile deformation energy, which results in the transition of the serrated chip to the continuous chip.

(iii) A double-tool FE model is utilized for simulating the SEV cutting process. The wavy surface with low-frequency oscillation strongly affects the SEV cutting process by inducing the evident variations of cutting force amplitude, which make the chip have non-uniform serrations. The influence of the high-frequency wavy surface on the cutting force is not significant, whereas PSBI determines the development of the serrated chip with uniform serrations.

(iv) The stability of the SEV cutting process depends on the relative damping coefficient and the additional damping resistance. The former represents the effect of inherent damping of the tool system. In the high-speed cutting process, the SEV stability limit increases with the relative damping, which is mirrored in the disappearance of the PSBI in the chip formation. The latter is related to the geometric characteristics of tool-system like the cutting width. Tool SEV will get more stable with the larger additional cutting damping. In the case of the small additional damping, the small cutting width can induce the unstable SEV.

Acknowledgements

This work was supported by the National Nature Science Foundation of China (Grant numbers 11572337, 11772346).

References

1. Adnan, A.S. and S. Subbiah, Experimental investigation of transverse vibration-assisted orthogonal cutting of AL-2024. Int J Mach Tools Manuf 2010; 50(3): 294-302.
2. Sui, H., et al., Feasibility study of high-speed ultrasonic vibration cutting titanium alloy. J Mater Process Technol 2017; 247: 111-120.
3. E. Shamoto, N. Suzuki, R. Hino, Analysis of 3D elliptical vibration cutting with thin shear plane model, CIRP Ann-Manuf Technol. 2008; 57: 57-60.
4. J. Zhang, T. Cui, C. Ge, Y. Sui, H. Yang. Review of micro/nano machining by utilizing elliptical vibration cutting. International Journal of Machine Tools & Manufacture 2016; 106: 109-126.
5. M. Zhou, Y.T. Eow, B.K. Ngoi, E.N. Lim, Vibration-assisted precision machining of steel with PCD tools, Mater. Manuf. Process. 2003; 18: 825-834.
6. M. Zhou, B.K.A. Ngoi, M.N. Yusoff, X.J. Wang, Tool wear and surface finish in diamond cutting of optical glass, J. Mater. Process. Technol. 2006; 174: 29-33.
7. M. Xiao, S. Karube, T. Soutome, K. Sato, Analysis of chatter suppression in vibration cutting, Int. J. Mach. Tools Manuf. 2002; 42: 1677-1685.
8. M.H. Miguélez a,n, X. Soldani a, A. Molinari. Analysis of adiabatic shear banding in orthogonal cutting of Ti alloy. International Journal of Mechanical Sciences 2013; 75: 212-222.
9. K. Liu, X.P. Li, M. Rahman, Characteristics of ultrasonic vibration-assisted ductile mode cutting of tungsten carbide, Int. J. Adv. Manuf. Technol. 2008; 35: 833-841.
10. Guillem Quintana a, Joaquim Ciurana. Chatter in machining processes: A review. International Journal of Machine Tools & Manufacture 2011; 51: 363-376.
11. M. Siddhpura and R. Paurobally. A review of chatter vibration research in turning. International Journal of Machine Tools & Manufacture 2012; 61: 27-47.
12. Das, S. Tobias, The relation between the static and the dynamic cutting of metals, International Journal of Machine Tool Design and Research 1967; 7: 63-89.
13. W. Knight, Application of the universal machinability chart to the prediction of machine–tool stability, International Journal of Machine Tool Design and Research 1968; 8: 1-14.
14. J. Tlusty, M. Polacek, The stability of machine tools against self-excited vibrations in machining, in: Proceedings of the International Research in Production Engineering Conference, Pittsburgh, PA, ASME, New York, 1963; 465-474.
15. J H.E. Meritt, Theory of self-excited machine–tool chatter, Trans ASME J Eng Indus. 1965; 87: 447-454.
16. J. Tlusty, Analysis of the state of research in cutting dynamics, Annals of CIRP. 1978; 27: 583-589.
17. Mahnama, M. and M.R. Movahhedy, Prediction of machining chatter based on FEM simulation of chip formation under dynamic conditions. Int J Mach Tools Manuf. 2010; 50 (7): 611-620.
18. Y. Gao, R. Suna, J. Leopold. Analysis of cutting stability in vibration assisted machining using an analytical predictive force model. 15th CIRP Conference on Modelling of Machining Operations Procedia CIRP 2015; 31: 515-520.
19. L. Vela-Martínez, J. C. Jáuregui-Correa, O. M. González-Brambila, G. Herrera-Ruiz, A. Lozano-Guzmán. Instability conditions due to structural nonlinearities in regenerative chatter. Nonlinear Dyn 2009; 56: 415-427.
20. T. Mabrouki, J.-F. Rigal, A contribution to a qualitative understanding of thermo-mechanical effects during chip formation in hard turning. Journal of Materials Processing Technology 176 (2006) 214-221.
21. M.N.A. Nasra, E.-G. Nga, M.A. Elbestawi, Modelling the effects of tool-edge radius on residual stresses when orthogonal cutting AISI 316L. International Journal of Machine Tools & Manufacture 47 (2007) 401-411.
22. Fei Shuang, Xiangyu Chen, Wei Ma. Numerical analysis of chip formation mechanisms in orthogonal cutting of Ti6Al4V alloy based on a CEL model. Int. J. Mater Form. Jan. 2017; DOI 10.1007/s12289-017-1341-z.
23. Al-Athel KS, Gadala MS., The use of volume of solid (VOS) approach in simulating metal cutting with chamfered and blunt tools. Int J Mech Sci. 2011; 53: 23-30.
24. Lee S, Lin CF., High-temperature deformation behavior of Ti6Al4V alloy evaluated by high strain-rate compression tests. J Mater Process Technol. 1998; 75: 127-136.
25. Z. Sun, F Shuang, W Ma. Investigations of vibration cutting mechining of Ti6Al4V alloy. Int J Mech Sci. 2018; 148:510-530.
26. Wu, D. W. and Liu, C. R., An analytical model of cutting dynamics. Part 2 Verification. Trans ASME J Eng. Ind. 1985; 107: 112-118.
27. Kudinov, V. A. et al. Experimental investigation of the nonlinearity of the dynamic characteristic of the cutting process. Translated by M. M. Barash, Stanki I Instrument 1978; 49: 11-13.
28. A. Moufki, A. Devillez, M. Segreti, D. Dudzinski. A semi-analytical model of non-linear vibrations in orthogonal cutting and experimental validation. Int J Mach Tools Manuf. 2006; 46: 436-449.